Supplementary materials for

Fabrication of porous TiO_2 nanorod arrays photoelectrodes with enhanced photoelectrochemical water splitting by helium ions implantation

Yichao Liu,[a] Shaohua Shen,[b] Fen Ren,*[a] Jianan Chen,[b] Yanming Fu,[b] Xudong Zheng,[a] Guangxu Cai,[a] Zhuo Xing,[a] Hengyi Wu[a] and Changzhong Jiang*[a]

[a]School of Physics and Technology, Center for Ion Beam Application and Center for Electron Microscopy, Wuhan University, Wuhan 430072, China.

[b]International Research Centre for Renewable Energy and State Key Laboratory of Multiphase Flow in Power Engineering, Xi'an Jiaotong University, Shanxi 710049, China.

* Corresponding authors.

E-mail addresses: fren@whu.edu.cn (F. Ren), czjiang@whu.edu.cn (C.Z. Jiang).

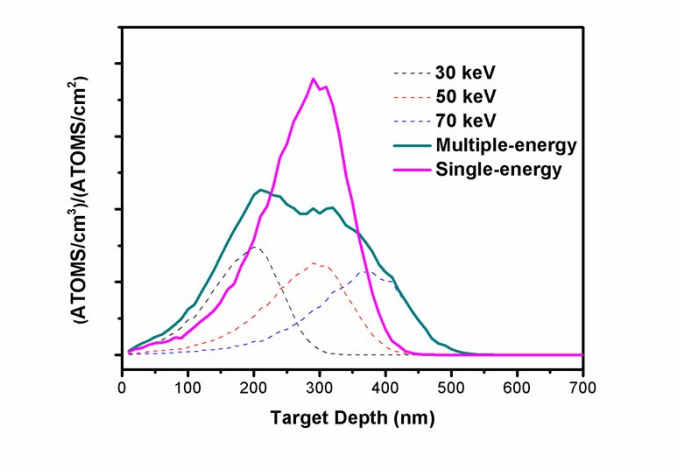

Fig. S1 Helium distribution in single energy (keV) and multiple energy (30, 50, 70 keV) helium ion implantation at total fluence of 3.35×10^{16} ions/cm^2, which were simulated by SRIM 2008.

Fig. S1 shows the distributions of the helium atoms in TiO_2 NRAs under multiple energies implantation. The projected ranges (Rp) of helium ions in the TiO_2 NRAs were calculated by SRIM 2008 for each ion energy, which are 173, 264 and 341 nm for the energies of 30, 50 and 70 keV, respectively[1]. The implantations were performed at room temperature, with the helium implanted vertically into the TiO_2 nanorod arrays in the form of He^+. To study the influence of size and number of nanocavities on the photocurrent, uniform size of nanocavities is needed. The following figure shows the SRIM simulated helium distribution in TiO_2 through multiple energy and single energy helium ion implantation. The aim of the multiple-energy helium ion implantation with several different energies and fluences is to create a relatively uniform helium concentration and to form uniform nanocavities in the nanorods. While for the single-energy ion implantation, the concentration of helium in TiO_2 nanorod arrays has a Gaussian distribution, where at the depth of the projected ranges (Rp), the concentration is relatively high, which leads to the formtion

of large nanocavities. According to our results, if the size of nanocavities is too large (sample 3A), the photocurrent will be decreased. Therefore, the TiO_2 nanorods with suitable size and uniform distributed porous structure perform better photocatalytic activity.

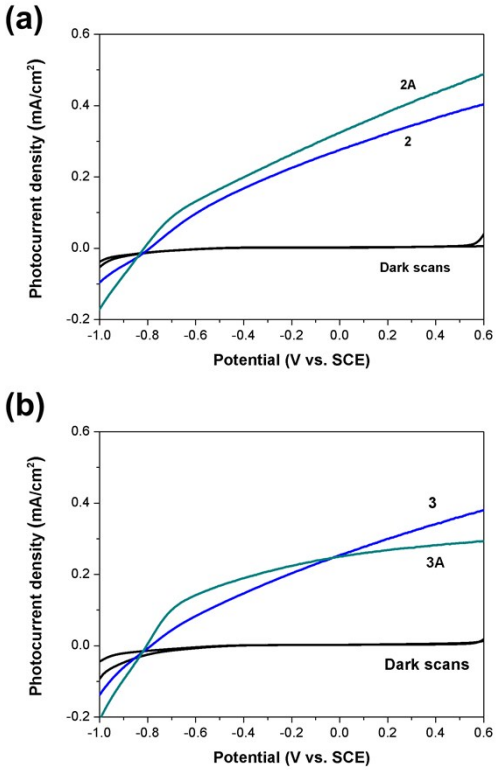

Fig. S2 The linear sweep voltammograms of the sample 2, 3, 2A and 3A, respectively.

Fig. S3 shows the schematic illustration of the amended increasing ratio for the porous TiO_2 NRAs of sample 1A. The total length of the TiO_2 nanorod is 3.7 μm, and the implanted layer is 682 nm. The measured photocurrent density of sample 1A is 2.63 times higher than the pristine TiO_2 NRAs, but the amended increasing ratio of the implanted layer B of the sample 1A is about 10 times higher than the same length A of the pristine TiO_2 NRAs.

In figures 1(a) and 1(b), we present the original measured photocurrent densities of all the samples. The measured photocurrent density of the sample comes from two parts

of the nanorods: the implanted region B and the non-implanted region C. The original measured data can not fully and truly reflect the role and contribution of nanocavity to the enhancement of photocurrent. Therefore, the amended increasing ratios of the photocurrent densities of the implanted and annealed samples are shown in figure 1(d). We assume that each unit length of TiO_2 has the same contribution to the whole photocurrent of the nanorod. Based on this assumption, we divided the nanorod into the two parts: the implanted region and the non-implanted region, the former is in 682 nm with 0.184 percent of whole length, and the rest takes the 0.816 percent. The photocurrent density of the pristine TiO_2 nanorod is 0.19 mA/cm^2, and the photocurrent density for unit length of TiO_2 nanorod is 0.19/3.7 $mA/cm^2/\mu m$. Thus, the contribution of non-implanted region to the total photocurrent can be obtained, that is 0.155 mA/cm^2 ((3.7 μm-0.682 μm)×0.19/3.7 $mA/cm^2/\mu m$). Therefore, we can calculate the contribution of implanted region for different implanted and annealed samples. For example, for the sample 1A, the measured photocurrent density is 0.5 mA/cm^2, the contribution of implanted region can be calculated to 0.345 mA/cm^2 (0.5-0.155 mA/cm^2). The amended increasing ratio of the photocurrent densities for the implanted region of this sample comparing to that of the 0.682 nm length of non-implanted region is 9.86 ((0.5-0.155)/(0.19-0.155)). The amended increasing ratios of rest samples are shown in the table 2. We acknowledge that such calculation may not complete accurate, but it more really reflect the influence of ion implantation.

We modified some sentences in the revised manuscript about the amended increased ratio of the photocurrent densities.

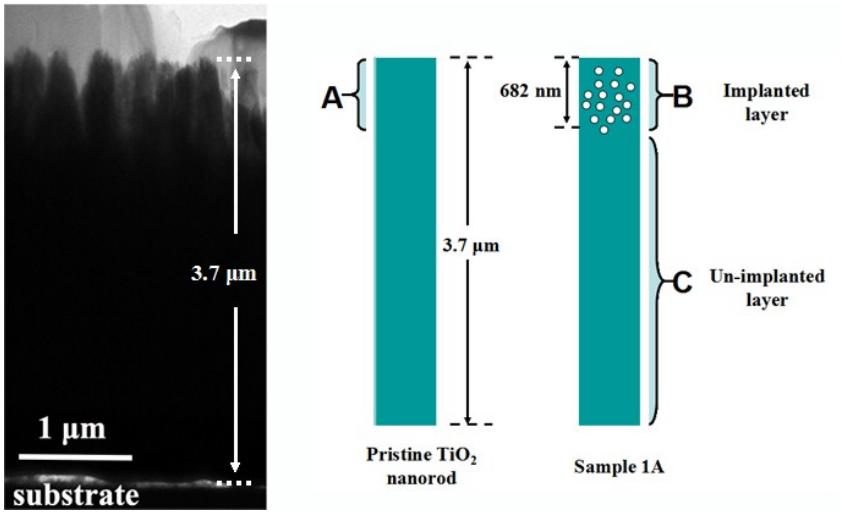

Fig. S3 The schematic illustration for calculation of the amended increasing ratio of the porous TiO_2 NRAs.

Table 2

Sample name	Photocurrent (mA)	Measured increasing ratio	Amended increasing ratio
TiO_2 NRAs (pristine)	0.19		
1	0.25	1.32	2.714
1A	0.50	2.63	9.860
2	0.38	2.00	6.430
2A	0.46	2.42	8.714
3	0.36	1.89	5.857
3A	0.28	1.47	3.571

Note: Measured increased ratio get from Photocurrent / 0.19 (I / I_0, I_0 = 0.19 mA), and the amended increasing ratio come from equation (I-0.155) / (0.19-0.155).

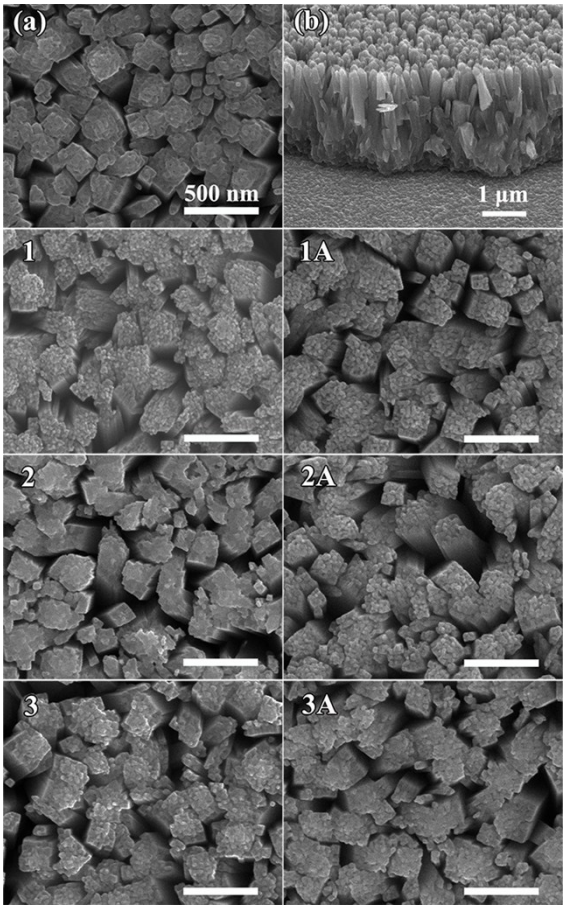

Fig. S4 SEM images of the TiO_2 NRAs on FTO glass implanted with different helium fluences and thermal annealing samples.

The broad emission band is observed which can be resolved to two peaks, as shown in figure S5. The peak centered at about 580 nm is ascribed to the oxygen vacancies or other defect states in the NRAs. The peak centered at about 660 nm might be a consequence of polarizability of lattice ions surrounding the vacancy [2-3].

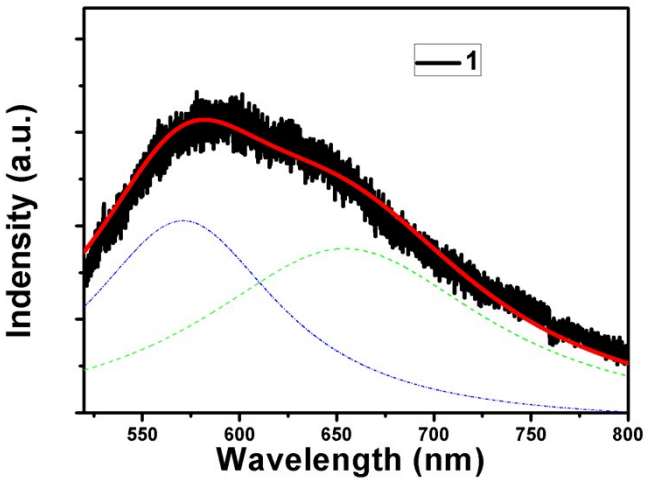

Figure S5. The photoluminescence (PL) spectrum of the sample 1

The electrical resistances of TiO_2 photoanodes were obtained by electrochemical impedance spectroscopy (EIS) in CHI 660D electrochemical workstation (as shown in the Figure S6). The frequency range is from 100 to 10^5 Hz and the open circuit voltage is 0.75 V. The results show that the pristine rutile TiO_2 NRAs have higher electrical resistance,[4] which leads to its worse PEC properties. While the samples 1and 1A have obviously lower resistance than that of the pristine TiO_2 NRAs. The EIS Nyquist plot under illumination conditions confirmed that the sample 1A photoanode possessed higher charge transfer rate and electrical conductivity than that of the pristine TiO_2 NRAs. It is further demonstrates that the trapping of holes by nanocavities to decreases the recombination of charge carriers, which takes the main responsibility for the enhanced PEC water splitting performance for the sample 1A.

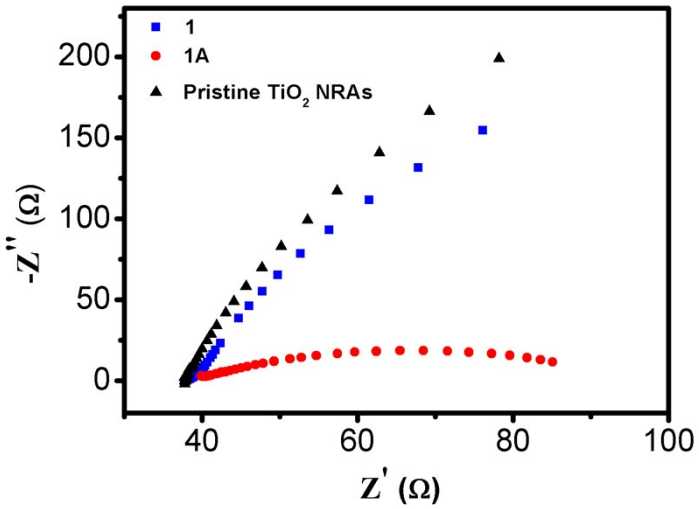

Figure S6. Nyquist plots of electrochemical impedance spectroscopy (EIS) measurements on TiO_2 nanorod electrodes before and after helium ion implantation, electrolyte: 1 M NaOH. Key: (▲) the pristine TiO_2 NRAs; (■) the sample 1; (●) the sample 1A.

It is known that the existence of vacancies will introduce a defect energy level in energy band structure of the TiO_2, which will increase the optical absorption of solar light.[5] The energy levels of vacancy in TiO_2 were reported to be 0.75 and 1.18 eV under the conduction band.[5-7] The E_{ov1} and E_{ov2} are referred to the oxygen vacancies (red dashed lines) that were induced by helium ion implantation and thermal annealing, as shown in the Figure S7. However, the band gap have not been narrowed in our experiment.

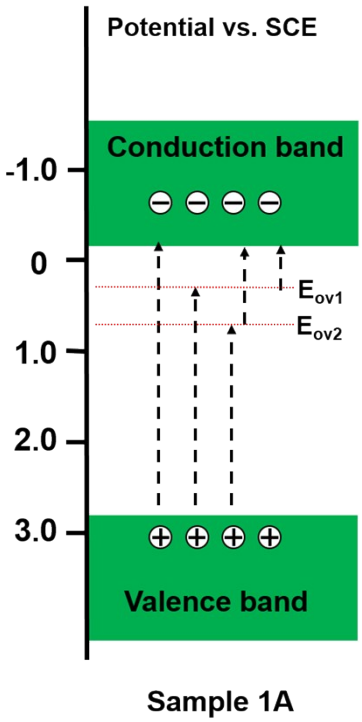

Figure S7. The illustration of defects energy levels in TiO_2 NRAs

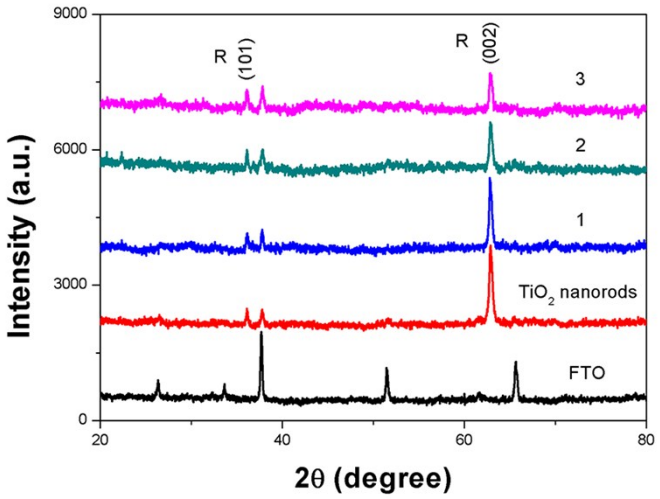

Fig. S8 XRD patterns of the TiO_2 NRAs on FTO glass implanted with different helium fluences.

Fig. S8 shows the XRD patterns of FTO substrate, the pristine rutile TiO_2 NRAs and the samples 1, 2 and 3, respectively. The intensity of peak (002) had a little decrease

as the increase of the helium implantation fluences, which accompanied a little crystal lattice damage by ion implantation. However, the TiO_2 NRAs still mainly in crystal rutile phase after ion implantation.

References

1 WWW. SRIM. org.

2 N. Serpone, D. Lawless, R. Khairutdinov, *J. Phys. Chem.*, 1995, **99**, 16646.

3 A.K. Ghosh, F.G. Wakim, R.R. Addiss, *Phys. Rev.*, 1969, **184,** 979.

4 Y. Yamada, Y. Kanemitsu, *Appl. Phys. Lett.*, 2012, **101**, 133907.

5 D. C. Cronemeyer, *Phys. Rev.*, 1959, **113**, 1222-1226.

6 D. C. Cronemeyer and M. A. Gilleo, *Phys. Rev.*, 1951, **82**, 975-976.

7 W. T. Kim, C. D. Kim and Q. W. Choi, *Phys. Rev. B*, 1984, **30**, 3625-3628.